Title

All polymer microfluidic chips-A fixed target sample delivery workhorse for serial crystallography.

Journal

Biomicrofluidics, 17(5)

ISSN

1932-1058

Authors

Gu, Kevin
Liu, Zhongrui
Narayanasamy, Sankar
et al.

Publication Date

2023-09-01

DOI

10.1063/5.0167164

Peer reviewed

Biomicrofluidics PERSPECTIVE pubs.aip.org/aip/bmf

All polymer microfluidic chips—A fixed target sample delivery workhorse for serial crystallography

Cite as: Biomicrofluidics 17, 051302 (2023); doi: 10.1063/5.0167164
Submitted: 10 July 2023 · Accepted: 27 September 2023 ·
Published Online: 13 October 2023

Kevin K. Gu,[1] Zhongrui Liu,[1] Sankar Raju Narayanasamy,[2] Megan L. Shelby,[2] Nicholas Chan,[1] Matthew A. Coleman,[2,3] Matthias Frank,[2,4] and Tonya L. Kuhl[1,a)]

AFFILIATIONS

[1]Department of Chemical Engineering, University of California at Davis, Davis, California 95616, USA
[2]Biosciences and Biotechnology Division, Lawrence Livermore National Laboratory, Livermore, California 94550, USA
[3]Department of Radiation Oncology, School of Medicine, University of California at Davis, Sacramento, California 95817, USA
[4]Department of Biochemistry and Molecular Medicine, School of Medicine, University of California at Davis, Sacramento, California 95817, USA

[a)]**Author to whom correspondence should be addressed:** tlkuhl@ucdavis.edu

ABSTRACT

The development of x-ray free electron laser (XFEL) light sources and serial crystallography methodologies has led to a revolution in protein crystallography, enabling the determination of previously unobtainable protein structures and near-atomic resolution of otherwise poorly diffracting protein crystals. However, to utilize XFEL sources efficiently demands the continuous, rapid delivery of a large number of difficult-to-handle microcrystals to the x-ray beam. A recently developed fixed-target system, in which crystals of interest are enclosed within a sample holder, which is rastered through the x-ray beam, is discussed in detail in this Perspective. The fixed target is easy to use, maintains sample hydration, and can be readily modified to allow a broad range of sample types and different beamline requirements. Recent innovations demonstrate the potential of such microfluidic-based fixed targets to be an all-around "workhorse" for serial crystallography measurements. This Perspective will summarize recent advancements in microfluidic fixed targets for serial crystallography, examine needs for future development, and guide users in designing, choosing, and utilizing a fixed-target sample delivery device for their system.

I. INTRODUCTION

X-ray crystallography has been the premier technique for protein structure determination, with over 170 000 structures obtained through x-ray crystallography deposited in the Protein Data Bank (PDB) to date.[1,2] The development of x-ray free electron lasers (XFEL) revolutionized x-ray crystallography, with the high brilliance of XFEL light sources making it possible to collect data from previously unusable protein microcrystals with conventional light sources.[3,4] The high intensity XFEL pulse yields detectable diffraction from a single exposure; however, the diffracting microcrystal is immediately degraded or destroyed (diffraction before destruction). This necessitated the development of serial femtosecond crystallography (SFX), in which single shots from thousands of randomly oriented microcrystals are used to collect a full rotational dataset.[5–7] Considered the new frontier for x-ray crystallography, serial crystallography techniques address the traditional bottleneck of obtaining large, well-diffracting protein crystals and eliminate the need for cryo-cooling to reduce radiation damage, allowing for the collection of more biologically relevant data at room temperature.[8–10]

Correspondingly, the advent of SFX required innovation in sample delivery methods, namely, ways to deliver numerous, delicate protein crystals to the beam interaction point at speeds accommodating the XFEL repetition rate. With thousands of microcrystals needed to obtain a protein structure with SFX, significant efforts have been made to identify optimal sample delivery methods that reduce sample consumption and time required to collect data.[11–16] A number of sample delivery methods have been developed, the first being gasdynamic virtual nozzles (GDVNs).[17,18] Early successes

using GDVNs for protein structure determination were achieved; however, GDVNs faced major limitations due to nozzle clogging and high sample consumption.[11,16,19–21] To address these issues, alternative methods were advanced, including droplet injectors,[22–24] electrospray aerosol generators,[25,26] and viscous media injectors such as agarose and lipidic cubic phase (LCP) injectors.[27–30] Nevertheless, their complex setup, operation and strict sample requirements have limited these methods' potential as a "workhorse" sample delivery method. On the other hand, fixed-target (FT) delivery systems, in which protein crystals are held in a sample holder and rastered through the x-ray interaction point as shown in Fig. 2, are notable for reduced sample consumption and improved ease of use. FT systems were often thought unsuitable for high-repetition rate experiments and restricted in the range of experiments due to limitations in sample scan speeds, use of high background sample supports, dimensional restrictions, or complicated loading requirements. In this work, we present new innovations in FT sample delivery that are easily, rapidly, and inexpensively fabricated, easy to use, and demonstrate relatively low background and high adaptability for a variety of experimental conditions and sample geometry requirements. The described FT is robust and well suited for SFX structure determination as well as for screening crystals under different conditions while minimizing sample requirements. To promote adoption by structural biology groups, we provide guidance to carry out successful synchrotron or SFX experiments using this "workhorse" sample delivery system and are especially well suited for screening crystals under different conditions while minimizing sample requirements. We also identify and discuss areas for innovation and improvement within FT sample delivery methods.

II. MICROFLUIDIC FIXED TARGETS FOR PROTEIN SERIAL CRYSTALLOGRAPHY

Fixed-target (FT) sample delivery methods at XFELs have been the focus of steadily increasing research interest, and several different FT devices have been developed within the last decade, including nylon loops,[31] microgrids, and microfluidic chips.[32–38] These FTs are then mounted in the path of the x-ray source and translated with motors to collect diffraction data from crystals inside or on the FT (Fig. 1). FT's offer advantages over other sample delivery methods, including low sample consumption, maintenance of the sample environment, option for *in situ* crystallization,[39] and the high degree of modularity of each sample-containing target, eliminating the need for lines, pumps, and other "plumbing" that increases sample-exchange time. A wide range of FT designs have been explored, notably microfabricated silicon or silicon nitride substrates,[35,40–43] which offer low scatter background, high x-ray transmission, and dimensional precision in their fabrication methods. However, microfabricated silicon or silicon nitride FTs are fragile, expensive, have longer fabrication lead times, are difficult to sample load and maintain sample hydration, and require ultrahigh precision FT translation. There can also be issues with x-ray beam damage and subsequent detector damage from silicon scattering if misalignment of the FT to the incident beam occurs. Other polymeric film materials, such as polyimide (Kapton),[44,45] Mylar,[46] and cyclic olefin copolymer (COC)[33,47] have also been developed, providing low x-ray absorption with easier

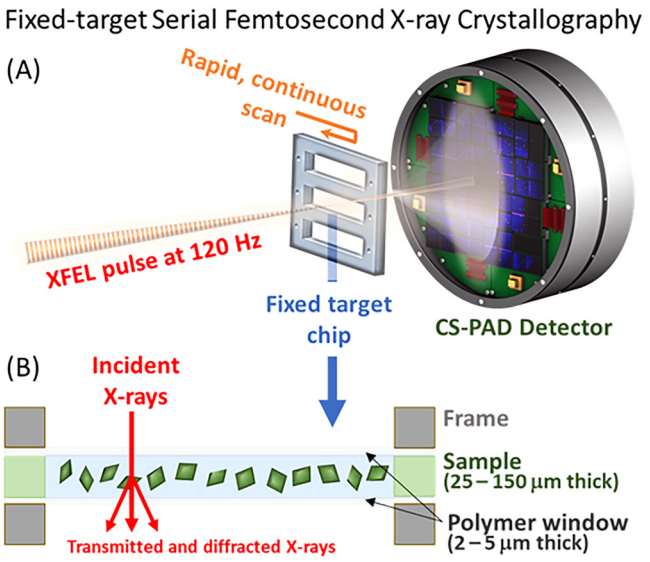

FIG. 1. (a) Schematic of a fixed-target x-ray serial crystallography experiment at Linac Coherent Light Source (LCLS). (b) Cross-sectional view of the fixed-target.

fabrication and usage. Microfluidic FTs consist of enclosed microfabricated or micropatterned solid matrices, in which either microliter volumes of crystal slurry are loaded or microcrystals are grown within the FT itself (Fig. 2). The integration of microfluidics facilitates incorporation of additional features,[55] such as controlling crystal locations,[38,48–51] complex *in situ* crystallization conditions,[52–58] adaptation for membrane protein crystallization via an LCP matrix,[59–61] and high-precision delivery flows.[62,63] However, the need to combine low background polymeric films, easy fabrication, and simple sample loading has limited the adoption of FTs as a "workhorse" sample delivery system for serial crystallography.

Ideally, a "workhorse" FT delivery system should exhibit certain features, such as

(1) Low background scatter to maximize signal to noise ratio.
(2) Easy crystal loading to minimize environmental stresses with stable storage conditions to maximize diffraction quality.
(3) Maximize data collected from available sample volume.
(4) Suitable for both high-repetition XFEL measurements and pseudo-serial synchrotron measurements.
(5) Easily modifiable for a variety of beamline requirements and sample considerations.
(6) Easily fabricated with accessible methods for a low barrier of entry.

In this Perspective, we discuss the design and usage of a specific microfluidic FT device conceptualized by our group to address common shortcomings of previous generation FTs, which we will refer to as a "chip." We believe that our chip meets all the basic requirements for an easy-to-use, general workhorse tool for serial

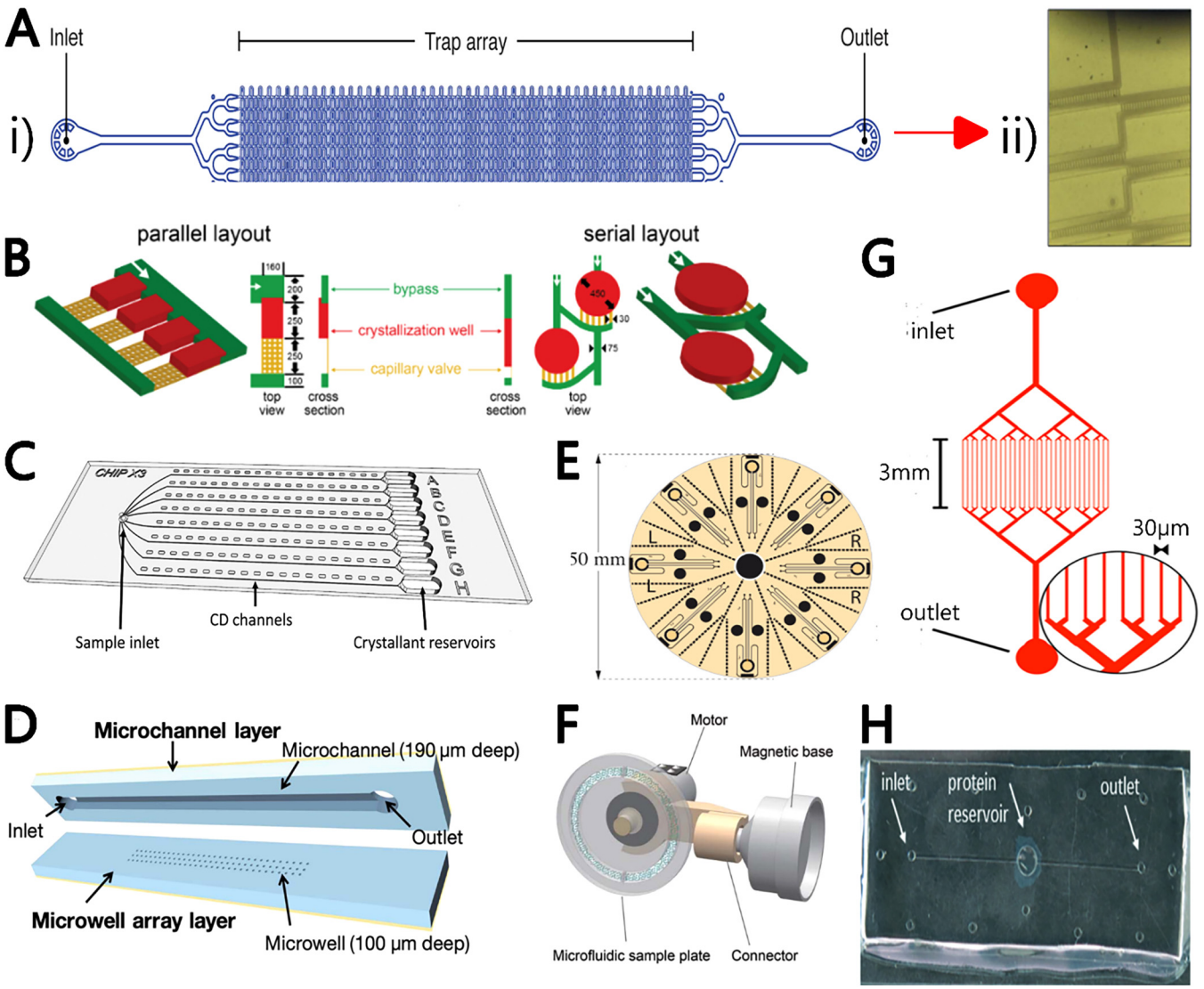

FIG. 2. Recent microfluidic FT designs for *in situ* serial crystallography. (a) Trap array designs. (i) Protein microcrystals are trapped in alternating weir-type arrays.[38] (ii) Simplified trap design based on (i).[48] (b) Microfluidic design using capillary valving to split aqueous reactions into nanoliter droplets for crystallization.[49] (c) ChipX3 designed for counter-diffusion screens of crystallization conditions.[50] (d) Microfluidic FT designed with modifiable microwell diameters to trap crystals by size.[51] Protein–ligand complexes are obtainable by refilling with ligand solution. (e) Centrifugally actuated microfluidic device to control fluid flow and enable metering for counter diffusive protein crystallization screens.[52] (f) Rotating FT device capable of three-degrees-of-freedom motion.[53] (g) Ultra-thin cyclic olefin copolymer (COC) microfluidic device with micrometer scale channels fabricated with UV-lithography and hot-embossing.[33] (h) FT integrated with cellulose dialysis membranes for crystallization by dialysis.[54]

x-ray crystallography experiments that is suitable for a wide range of applications.

A. Fabrication steps and design requirements

A schematic of the chip's layered assembly is shown in Fig. 3. In brief, 1 mm thick polymethyl methacrylate (PMMA) sheets (SimbaLux, 5 × 7 in.) were purchased from Amazon. An adhesive is applied to one side of the PMMA sheet using an adhesive transfer tape (3 M, F9460PC). These frames are CO_2 laser cut to the desired design to form Layer 2. Cyclic olefin copolymer (COC; TOPAS Advanced Polymers Grade 6017, T_g= 170 °C) films are obtained by spin coating a solution of COC in sec-butylbenzene on a silicon wafer. The PMMA frames are then adhered to the COC film directly onto the wafer and removed using a lift-off process (layers 2 and 3). Symmetric assembly of layers 2 and 3 are

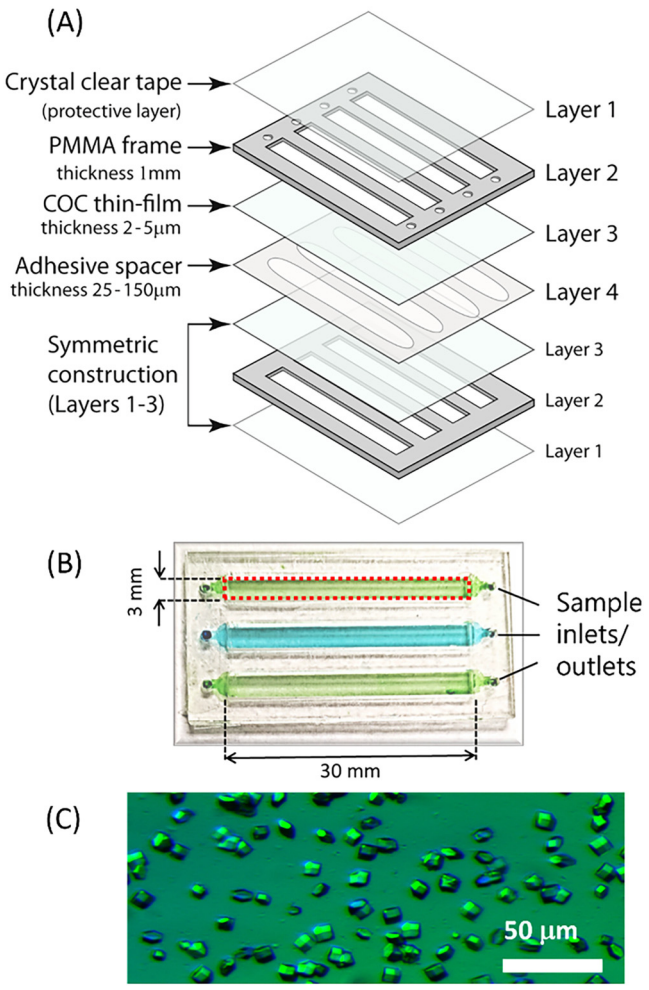

FIG. 3. (a) Schematic of the individual layers of the all-polymer microfluidic chip for fixed-target serial crystallography. (b) Image of an assembled chip with three independent x-ray imaging areas. (c) Optical microscope image of lysozyme crystals grown on chip and used to determine the structure of lysozyme to 1.7 Å at the LCLS, MFX beamline. Adapted from Liu *et al.*[64]

connected by a double-sided adhesive (layer 4; Adhesives Research, ARcare® 92712) and aligned by hand. To protect the COC films during transport, handling, etc., Duck® Brand HP260™ packing tape is placed over both sides of the chip. Detailed fabrication steps and techniques are provided in Liu *et al.*[64] The design features large area, few micrometers thick, polymer windows that have low x-ray scatter to enclose the crystal sample. Independent microfluidic channels (windows) allow for loading of unique samples or crystallization conditions within the same chip. Within the bounds of this fabrication, several parameters can be adjusted to meet sample or beamline requirements, including overall chip dimensions and shape, imaging window dimensions and shape, channel or sample flow layer thickness, inlet design, and chip materials.

There are numerous advantages of using only amorphous polymers in the fabrication. Key points are summarized here. First, polymer materials are inexpensive, easy to work with, and amorphous polymers have relatively low scatter background from the imaging window. Second, precise x-ray beam alignment during high-repetition rate XFEL measurements is not necessary. The all-polymer FT chip is simply rastered at a constant speed to obtain a desired shot spacing. X-ray shots that hit the 1 mm thick frame contribute a high scatter background but do not generate high intensity Bragg peaks associated with ordered material, thereby minimizing the risk of damage to the x-ray area detectors. Furthermore, frame-intersecting shots are filtered out during data analysis by their unique scattering profile. Third, the chip, and described storage holder, can maintain sample stability for weeks or more. Under ambient conditions, lysozyme crystals have been observed to be stable for up to 10 days, while we believe chips stored in the described storage holder can last for months or more. Fourth, the use of transparent materials means users can use conventional microscopy to *a priori* optimize sample quality and ultimately select chips with high sample quality for synchrotron or XFEL measurements.

1. Material selection

The chip design presented here consists of three main material components, the frame, thin film window, and adhesive spacer, which defines the microfluidic sample layer. Materials selection for FT sample delivery involves a few specific considerations, such as x-ray and optical transparencies, mechanical properties, water permeability, and fabrication requirements.

Key components of the device that require optimization of material properties are the materials in the x-ray beam path. We selected cyclic olefin copolymer (COC) as the thin film window material [Layer 3, Fig. 2(a)], owing to its low contribution to background scatter, relatively low water permeation rate, and the ability to easily form controllable micrometer-thick films by simple spin coating.[47] COC film thickness is controllable as a function of spin speed and solution concentration.[64] COC has a 99% transmission at a thickness of 8.9 μm for an x-ray beam of 12.4 keV, demonstrating low x-ray absorption or scattering due to the COC film.[55] We have also explored other materials, such as epoxy, to produce films with improved mechanical properties that are robust for larger continuous window areas without film sagging but have a higher water permeability. A unique aspect of the fabrication is the use of commercial hydrophilic double-sided adhesives for the sample channel/spacer material (layer 4). The adhesive used in this work consists of a polyester substrate and acrylic adhesive that was laser cut to match the dimensions of the PMMA frame. Strong adhesion between the window film material and adhesive spacer is required to maintain structural integrity and reduce hydration loss. A variety of double-sided adhesive layer thicknesses with different physical properties are commercially available to meet various sample requirements. Thick sheets of polymethylmethacrylate (PMMA, layer 2) provide structural support to the thin polymer film and sample layer. Finally, the whole chip is sealed with clear packing tape (layer 1) to protect the thin COC windows during handling and transport, seal the inlet and outlet holes, and decrease

evaporation from the chip. The protective crystal clear tape is removed from the x-ray imaging area prior to x-ray diffraction measurements and is not required when the chip is placed in long-term storage as described in Sec. II C.

2. Adjustable dimensions

Previous FT devices have required photolithography or other complex fabrication techniques, making device design and dimension changes more difficult, time consuming, and costly. Simple fabrication methods enable quick turnaround times for a wide range of design modifications. For example, changes in FT dimensions are often necessary to meet specific beamline or sample requirements. With our simple fabrication method, changes in overall chip dimension, window geometry, and inlet/outlet design can be fabricated in a single day using commonly available equipment. Specifically, the dimensions of the chip (Fig. 3) are simply controlled by CO_2 laser cutting the PMMA frame (layer 2) and adhesive spacer/channel flow layer (layer 4) to the desired dimensions. The thickness of various chip components is guided by sample requirements. The sample thickness orthogonal to the x-ray beam is determined by the thickness of layer 4 (typically, 25 or 48 μm) and the thickness of the COC window film (layer 2). For 2–3 μm thick COC windows, easily prepared by spin coating, the maximum free standing film width is about 3.5 mm with any length desired for the channel. Larger widths can be problematic due to opposing window film contact prior to sample loading. Thinner COC windows will reduce background scattering with a concomitant increase in the sample dehydration rate; however, background scattering is primarily from excess crystallization buffer in the x-ray beam—sample cross section.[55] To limit diffuse scatter from the buffer during crystal hits and prevent crystal displacement during measurements, the channel flow layer should roughly match the dimensions of the protein crystal. The sample flow layer can be easily adjusted by applying double-sided adhesive (layer 4) of desired thicknesses. The thickness of commercially available adhesives ranges from 25 to 150 μm, matching the range of crystal sizes used in serial crystallography. If thinner sample flow layers are desired, a commercially available 13 μm thick COC sheets can be physically cut or a COC sheet can be hot embossed as in our previous work.[32]

B. Protein sample

The emergence of SFX has led to a shift in ideal protein sample characteristics. Instead of cryo-cooled singular large, well-diffracting crystals, SFX experiments focus on room temperature collection from a high density of small microcrystals.[65–68] Due to the limitations in XFEL availability, judicious planning to grow crystals of the optimal size, diffraction quality, orientations, while maintaining sample stability is needed to maximize resultant data collection efficiency and data quality.[69,70] A distinct advantage of microfluidic FT approaches is the ability to accommodate a variety of crystal sizes and morphologies. Larger microcrystals (>30 μm) in the FT can be measured at synchrotrons.

1. On-chip crystallization

In situ protein crystallization is possible in microfluidic FT sample delivery devices. The described chip works with microbatch or vapor diffusion crystallization conditions. For microbatch, the FT inlet and outlet holes are sealed with Hampton crystal clear tape. For vapor diffusion, the inlet and outlet holes are left unsealed to allow slow exchange of water vapor. The chip is then placed in an enclosure with a reservoir of crystallization buffer. Relative humidity (RH) can be controlled during storage to adjust the water evaporation rate during on-chip crystallization.

For on-chip crystallization, the chips are typically loaded with a well-mixed 1:1 solution of protein and precipitant solution by gently pipetting into one of the inlet holes. The volume of solution needed to fully fill the flow channel is determined by the dimensions of the adhesive sample flow layer—for example, in Fig. 3 the 3 mm × 30 mm × 48 μm channel requires 4.5 μl of the solution. Although alterations in crystallization are to be expected for crystallization on-chip compared to off-chip methods, for soluble protein on-chip crystallization, similar crystal sizes and morphologies were obtained without modifications to established crystallization conditions.[32] However, slow water evaporation rates and low Grashof number conditions on chip result in slower crystal growth rates. There is also a decrease in the nucleation rate due to the large interfacial contact between the thin film and the sample layer and a reduction of natural convection around crystals in channel heights of less than 100 μm.[71] These aspects can be advantageous for obtaining larger crystals in FTs and concomitant reduction in the buffer background. Preferential orientational growth is possible in microfluidic channels due to the reduction of natural convection of solute, causing areas of depletion around crystals in channel heights of less than 100 μm.[71] Fortunately, the large FT x-ray imaging window accommodates a wide rotational angle.

2. Slurry loading

A significant advantage of microfluidic FTs is the ability to slurry load samples. Proteins that are difficult to crystallize require specialized crystallization procedures, or proteins with minimal sample volume grown with other techniques can be loaded with their surrounding mother liquor into the FT by micropipette. The dimensions of the channel and volume in an imaging window channel can be matched to the protein sample and volume limitations. It is imperative that the channel height be close to the crystal sizes to reduce background, minimize crystal motion during stage movements, and settle due to gravitational effects.[11] Crystal displacement is especially evident when rotating the sample during serial synchrotron measurements (Fig. S2 in the supplementary material). High viscosity crystallization conditions containing large amounts of PEG or other viscosity-increasing additives can be used to minimize the crystal motion.

For example, one option for increasing sample viscosity and long-term sample storage stability is the addition of Pluronic F-127 (PF-127), a non-ionic surfactant composed of polyoxyethylene–polyoxypropylene copolymers.[72] At concentrations between 20% and 35% (w/v) PF-127 forms a thermoreversible gel, existing as a liquid at 4 °C and as a solid at room temperature.[73] Mixing PF-127 and a crystal suspension at 4 °C provides a liquid solution for crystal slurry loading into the chip. At room temperature, a solid

hydrogel matrix is formed to fix crystals in their initial locations while maintaining precise sample layer thickness. Using HVE injectors, Kovácsová *et al.* demonstrated PF-127's compatibility with protein diffraction measurements and resolved the structures of glucose isomerase, thermolysin, and bacteriorhodopsin to 2.0, 2.0, and 2.3 Å. Furthermore, they found PF-127 is chemically compatible with final concentrations of 0.25M ammonium sulfate, 2M NaCl, 25% (w/v) polypropylene glycol 400, 23% (w/v) polyethylene glycol 400, and 7% (w/v) polyethylene glycol 2000.[74] PF-127 may also help maintain protein crystal hydration under vacuum and long-term storage.

Finally, when slurry loading delicate, large (>50 μm dimension) uridine-specific nidoviral endoribonuclease (NendoU) crystals, which have needle or rod-like morphologies, significant crystal damage due to the high shear stress gradient was observed at the entrance to the sample flow channel. The maximum shear rate occurs at the constriction between the inlet hole and the narrow flow channel. When the crystal material strength is exceeded due to shear stress, the crystals fracture, leading to a decrease in the diffraction quality. We have not observed crystal damage when slurry loading large crystals of lysozyme, thaumatin, or Rapid Encystment Protein (REP) or when slurry loading smaller 10–15 μm crystals of NendoU or Photosystem I. To reduce the shear stress during slurry loading, a more gradual incline between the inlet hole in the PMMA frame and the sample flow layer can be obtained using a conical drill. Numerical analysis (see in the supplementary material) was used to estimate the shear rate during slurry loading with respect to lateral position for the two inlet designs, a "sharp" inlet with a perpendicular cross section between the inlet and the sample channel, and a "curved" inlet with a conical cross section to the flow layer. The shear rate is reported in Fig. 4 as a function of distance as the fluid traverses through the inlet channel, when it passes through the bend, and the imaging region where x = 0 corresponds to the leading edge of the chip. The shear rate is calculated from the gradient of the 3D cross-sectional velocity profile during fully formed flow in the center of the channel. At the "sharp" inlet, flow recirculation is observed, and the fluidic constriction increases the pressure gradient and, thus, the shear rate. In the case of the curved inlet shape, this fluidic constriction is minimized, resulting in a decrease in the shear rate. Under either case, i.e., sharp, or curved inlet, the shear rate settles to a relatively constant value as it flows through the imaging region with constant cross-sectional dimension, resulting in a uniform rectangular laminar velocity profile.

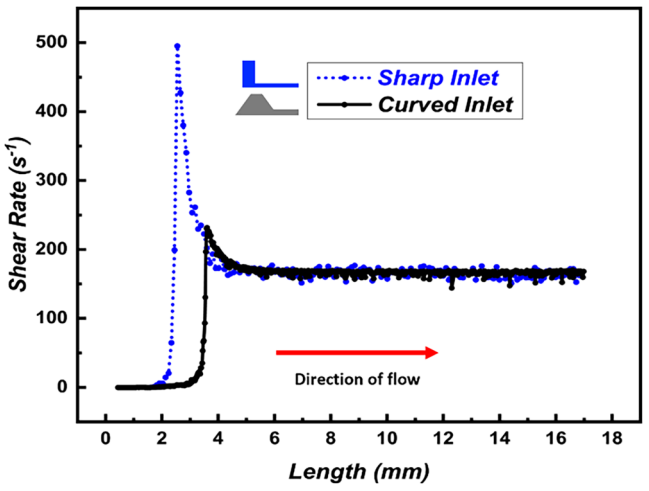

FIG. 4. Numerical analysis of the shear rate when loading at a rate of 0.5 μl/s for sharp and curved inlet designs for chips with a flow layer height of 48 μm. The x-axis is the distance from the first edge of the chip. The spike in the shear rate during loading at the inlet can be significantly reduced using the curved inlet design. Details on the numerical analysis and geometry can be found in the supplementary material.

3. Controlling crystal densities

An important consideration to optimize efficient data collection during FT-SFX experiments is ensuring a high density of crystals within the FT device. Higher crystal densities correlate to higher hit rates and faster data collection. The hit rate depends on a variety of factors, including crystal size, crystal agglomeration, crystal density, pulse repetition rate, shot spacing, and x-ray beam size. From the Poisson statistics calculated at densities of ~10^8 particles/cm^2 for 100 nm sized samples with a 1 μm diameter x-ray beam, the optimal hit rate is ~37% for single crystal hits.[75] Higher hit rates can lead to multiple crystal hits, which can be an issue with small microcrystals or highly clustered crystals. A significant advantage of microfluidic FT sample delivery is control over crystal densities. When slurry loading, crystal density can be adjusted by concentrating or diluting the crystal slurry. Higher crystal densities can be obtained by leaving crystal suspensions to settle overnight or by gently centrifuging and collecting from the bottom of the microtube. For protein crystals grown *in situ*, crystallization conditions need to be optimized to reach desired crystal densities. Crystal density and size can be controlled to a degree in on-chip crystallization by adopting methods that increase the nucleation rate, most commonly by seeding. Introducing dilute micro–nano seeds prepared from crystals grown with conventional off-chip methods has proven an effective method to control the crystal size and density on-chip.[76]

C. Sample stability and storage

Due to the fickle nature of protein crystallization and the limited availability of XFEL beamtimes, it is ideal to prepare protein samples well before measurements are conducted. A clear advantage of microfluidic FT sample delivery systems is the ability to store samples for long periods of time. The thin window films used in our chips have low water permeability but changes in relative humidity (compared to the osmotic pressure in the sample loaded chip) will cause water transport into or out of the chip over time. Maintaining constant hydration and stable conditions within the chip is essential for maintaining protein crystal diffraction quality during storage.[77–79] Additionally, relative humidity and water loss are important factors for crystallization. The steady-state water vapor transmission rate (WVTR) as a function of COC film thickness allows optimization of crystallization conditions.[32] As a part of our goal of making FT sample delivery user-friendly, we have also developed means to maintain sample stability for weeks

to months. This is simply achieved by placing sample loaded FTs in air-tight acrylic cases. The cases are fabricated to minimize the free volume that equilibrates with the chip. Instead of trying to control relative humidity and temperature, the sample simply equilibrates with the small free volume, thereby minimizing changes in sample hydration. Importantly, the FTs and contained crystal samples can be monitored *in situ* using optical microscopy. Long-term stability also greatly facilitates screening multiple crystal samples and conditions as there is very little downtime associated with FT sample changes.

The key to long-term storage of protein crystal samples depends on maintaining crystal hydration. While evaporation rates through the FT film material are slow enough to limit water loss during data collection, samples will dry out within days without any environmental controls. Traditionally, water loss due to evaporation is controlled by equilibration of relative humidity (RH) inside a sealed container. Salt solutions in these sealed containers can be used to maintain RH conditions, but recipes that need to be adjusted are dependent on the actual concentration of the sample in the chip and temperature, which sets the RH. Conversely, one can simply maintain hydration under any conditions by minimizing the free volume. This limits the amount of liquid needed to evaporate in order to reach the saturation point of water. An acrylic chip storage chamber was designed and fabricated to meet this requirement (Fig. 5), with an inset volume slightly greater than the volume of an assembled chip. This leaves the free volume outside the chip equivalent to the volume of the cutout PMMA frame, approximately 700 mm^3, which accounts for three $3 \times 30\ mm^2$ sample windows, the two sides of the 1 mm thick PMMA frame $3{\times}3\ {\times}30\ {\times}1\ mm^3 \times 2 = 540\ mm^3$, and the extra 0.5 mm around the FT. The calculation for water loss in weight % in the FT to keep 100% RH in the sealed storage chamber at 298 K and 1 atm conditions is given below:

$$\%W = \frac{m_{vaporized}}{m_{channel}} \times 100\%,$$

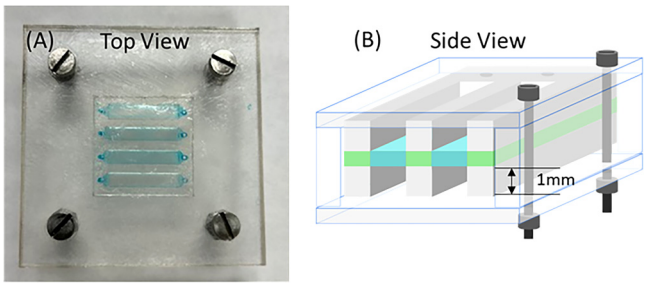

FIG. 5. (a) Image of the FT chip in the acrylic storage chamber. (b) Schematic of the storage chamber with chip. Acrylic is CO_2 laser cut with through holes for bolts. The chamber is composed of three different layers. The bottom is a solid 3 mm thick piece. The middle is a 3 mm thick piece with a center cut out that is 0.5 mm wider on all sides than the chip dimension. The top is a solid 1 mm piece for ease of optical imaging. The top is sealed with vacuum grease along the conformal portions. The middle and bottom can also be sealed this way or glued.

where $m_{vaporized}$ is the mass of water vapor in the excess volume at saturation vapor pressure and $m_{channel}$ is the mass of the water in the chip. The maximum mass of water vapor in a fully saturated volume is given by

$$m_{vaporized} = \frac{P_{sat} V}{RT} \times MW_{water},$$

where P_{sat} is the saturation partial pressure of water. A mere 0.12% of water from a chip is sufficient to reach 100% RH in the storage chamber at 25 °C. The storage chambers are effective, inexpensive, and independent, ideal for facilitating sample screening.

D. Data collection and measurements

1. Pseudo-serial crystallography at synchrotrons

The described microfluidic FT device has been demonstrated at both synchrotron and XFEL sources. Synchrotron measurements were conducted at the crystallography Beamline 12–1 at the Stanford Synchrotron Radiation Lightsource (SSRL). Individual FTs were imaged with the inline camera system and large, high-quality crystals were selected, centered, and measured using ±40° with 1° degree increments. Diffraction data were collected at ambient temperature using a wavelength of 0.979 Å, a beam size of $0.05 \times 0.04\ mm^2$, and an Eiger X 16 m detector (Dectris AG) at a detector distance of 0.2 m. No degradation of the FT was observed, and high-quality diffraction data were obtained, enabling high resolution structure determination to 1.5 Å of a variety of model proteins.[32,64]

Compared to other room temperature sample delivery techniques for serial crystallography (e.g., liquid or viscous media jets, which must be loaded with a freshly crystallized slurry or un-enclosed FTs that require onsite-loading and meticulous humidity control or cryo-freezing), minimal sample preparation is needed during beamtime from the perspective of the user. Chips can be assembled in advance; chips with crystal samples can be prepared beforehand and stored until data collection; empty chips can be slurry loaded in advance or right before data collection. Both on-chip crystallized samples and slurry loaded samples have been successfully characterized.[32,64]

Generally, many crystallography-oriented beamlines have specific setups for FT sample delivery, which include a goniometer to rotate the chip, translational motors to move the chip, and an inline camera. A standard, screw tightened, slotted holder with a magnetic base is used to mount the chip on the goniometer. Once a chip is mounted, a specific crystal is placed into the beam path by manually aligning the crystal using the inline camera and translational motors. Ideally, the identified protein crystal is larger than the beam spot size, with the beam spot focused on the identified crystal even during rotation. At SSRL, the *Blu-Ice* software package was used to control motor translation and rotation for crystal alignment. Rotational wedges for identified crystals were then collected. Since the most significant source of background scatter is from the aqueous layer, it is important to match the flow layer thickness to the size of the crystal since rotation will increase the path length of the aqueous layer. Diffraction analysis was performed during data acquisition to verify completeness. Typically, 10–20 crystals were

sufficient for data collection, depending on the rotation length, crystal quality, symmetry, and radiation sensitivity.[32,64]

2. Serial crystallography at XFELs

The chip was demonstrated for serial crystallography at the Macromolecular Femtosecond Crystallography (MFX) instrument at the Linac Coherent Light Source (LCLS), SLAC National Accelerator Laboratory (see Fig. S1 in the supplementary material).[80] Measurements were conducted at a photon energy of 9.89 keV, ~3–5 μm spot size, 120 Hz repetition rate, and a detector distance of 89.7 mm in a helium-rich ambient (HERA) environment to reduce background from air scattering. A 3D printed sample holder was designed to hold the microfluidic chip and mounted to MFX's translational motor system with screws. While running at a fixed pulse repetition rate, the shot spacing was controlled by adjusting the translational motor speed. Linear actuator operational velocities between 6 and 24 mm/s were used, giving tunable shot spacings between 50 and 200 μm. Optimal shot spacings can depend on several factors, including x-ray beam transmission, repetition rate, crystal density, potential shockwave propagation, and desiccation rate.

After mounting, data collection was conducted through a continuous raster scan through each window of the chip. A simple script was used to raster the chip at a specified speed for specified times, allowing for variations in shot spacing and rastering area. A 50 μm shot spacing was primarily used. Inline cameras were used to align the starting position of the script at the upper corner of the first sample channel. Since the chip is made of amorphous low-Z polymeric materials, misalignment was not an issue as pulses hitting the frame produced easily distinguishable high, average background patterns. Importantly, frame shots do not cause damage to the detector. A full chip scan of a chip at 120 Hz with 50 μm steps took about 20 min. In demonstration measurements, the structure of ~10 μm diameter lysozyme crystals was resolved to 1.7 Å using data collected from two 48 μm spacer FTs. The total sample volume was 24 μl and a mere 0.6 mg of protein.[64] However, this is not representative of the maximum resolution obtainable with the FT, as the resolution can be improved by matching the crystal size and sample thickness layer to better minimize background contribution. Overall, 29 215 indexed diffraction hits were obtained yielding ~13 indexed hits/s. The hit rate could be further improved with more precise alignment with the sample windows, maximized crystal density, and further insight into the minimum useful shot spacing. Future work will look in detail at maximizing x-ray shot density in the context of the potential of shockwave propagation and crystal damage or displacement caused by LCLS pulses on these FT systems.

The ability to refine a complete protein structure from 0.6 mg (~24 μl) of protein sample and ~45 min of total data collection time demonstrate the powerful potential of FT systems as a workhorse sample environment system for XFEL serial crystallography. Furthermore, the modularity of FT delivery dramatically reduces downtime during sample exchange, as new chips with entirely different samples (each channel in the chip is independent) can be quickly mounted once a raster scan is completed. Multichip platforms would further decrease downtime. This highly modular and easily-to-use microfluidic chip design will enable high-throughput serial crystallography experiments with minimal setup and a low barrier to entry.

3. XFEL data collection optimization

Despite the growing interest in FT sample delivery for SFX experiments, a few studies have been conducted to examine optimal experimental conditions for data collection. With the goal

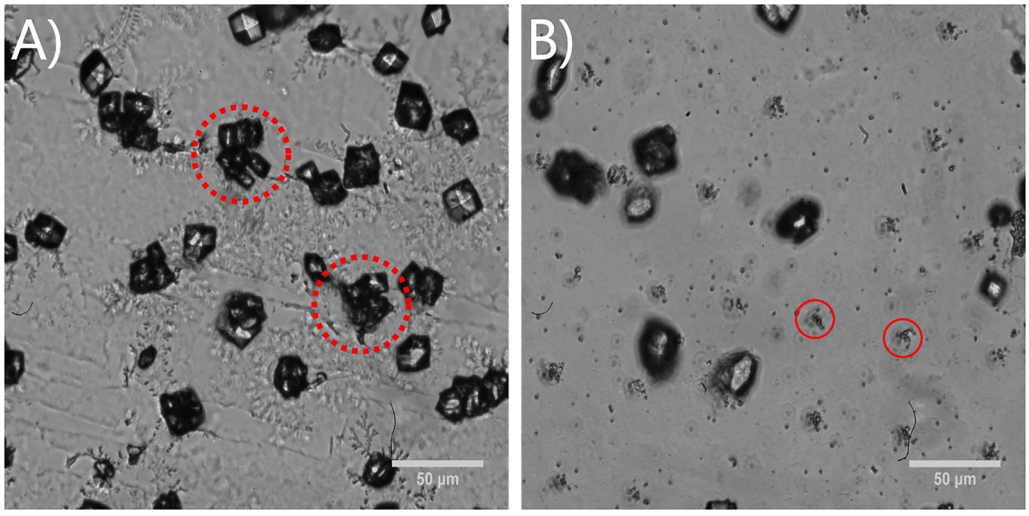

FIG. 6. Lysozyme crystals in the chip after XFEL data collection. (a) "Destruction" of crystals after x-ray exposure (red dashed circles). (b) Bubble formation after x-ray pulse exposure (red circles) at 11% transmission indicating distance between shots. Scale bar is 50 μm.

of using these technologies to study biologically relevant proteins, experimental efficiency is key to obtaining useful structural information from protein crystals with limited sample availability.

Due to the high energy character of XFEL pulses, secondary radiation damage events, potential shockwave propagation, and formation of vapor cavities may affect unexposed areas nearby, by causing the displacement of crystals, reduction of diffraction quality due to radiation damage, or crystal degradation due to imposed stress and hydration loss (Fig. 6).[21,81–85] The generation of shockwaves is dependent on the energy absorbed by the system, which is further dependent on the energy dependent cross-sectional x-ray absorption coefficients of the film, mother liquor, and crystal density.[86] In preliminary studies, chips with 48 μm sample thickness and about 10 μm crystals, 62.7% transmission, defined as the ratio of a number of photons over the maximum number of photons at LCLS, yielded high-quality diffraction data and no change in the hit rate during measurements. Observationally, at 80% transmission, significant bubble formation occurred and the hit rate decreased. At 100% transmission, damage to the film material occurred as rapid sample dehydration was observed during the measurement. Previous work has demonstrated the need to translate 30–100 μm between shots to contain the effects of beam damage on data quality.[9,35] Systematic studies with high-speed imaging of the sample at the x-ray beam intersection are scheduled in the future at LCLS to examine the specific mechanisms of damage propagation in these FTs to help researchers make more informed decisions on the effects of beam parameters on measurements. Furthermore, due to the high amounts of data produced during SFX experiments, statistically significant data analysis will be possible to validate the effects of transmission, shot spacing, beam profile, and wavelength on data quality and collection efficiency.

III. OUTLOOK

The described microfluidic, FT devices for serial crystallography at both synchrotron and XFEL light sources are easy to use, robust systems that can meet many protein crystallography needs while reducing the barrier to entry to users. We predict that current FT technologies are only scratching the surface of what is possible—experimental optimizations and incorporation of novel features will extend the efficacy and efficiency of FT serial crystallography. The modular and easily modifiable design of the described chips simplifies the inclusion of new features to meet different user needs and incorporate advancements in the field, including separating protein crystals by size,[87] trapping crystals in specific locations, adaptation for membrane proteins,[88–90] counter-diffusion crystallization,[91] compatibility with pump–probe experiments, and integration with electric fields.[92] Finally, while the feasibility of FT systems has been tested at 120 Hz and even up to 1 kHz,[93] FT viability at MHz repetition rates at the European X-ray Free Electron Laser (EU-XFEL) or LCLS-II still remains to be seen. Improvements in translational motor speed and resolution, inclusion of shockwave absorbing materials, and multi-chip sample holders may facilitate future low background, efficient, and damage-free MHz measurements using FTs. Overall, the flexibility and ease of use of FT systems drive its potential as a "workhorse" system to fully adopt the benefits of serial crystallography for protein structural characterization.

SUPPLEMENTARY MATERIAL

See the supplementary material for accompaniment figures for data collection at XFEL light sources and details regarding the simulation methodology for Fig. 4.

ACKNOWLEDGMENTS

This work was performed, in part, under the auspices of the U.S. DOE by LLNL under Contract No. DE-AC52-07NA27344. This work was supported by the National Science Foundation (NSF) BioXFEL STC Grant No. 1231306 and NIH Grant Nos. R01GM117342 (NIGMS) and U19 AI144184 (NIAID). Use of the Stanford Synchrotron Radiation Lightsource and Linac Coherent Light Source at the SLAC National Accelerator Laboratory is supported by the U.S. Department of Energy, Office of Science, Office of Basic Energy Sciences under Contract No. DE-AC02-76SF00515. The SSRL Structural Mole4culary Biology Program is supported by the DOE Office of Biological and Environmental Research and the National Institutes of Health, National Institute of General Medical Sciences (No. P30GM133894). The contents of this publication are solely the responsibility of the authors and do not necessarily represent the official views of the NIGMS or the NIH.

AUTHOR DECLARATIONS

Conflicts of Interest

The authors have no conflicts to disclose.

Author Contributions

Kevin K. Gu: Conceptualization (equal); Investigation (equal); Visualization (equal); Writing – original draft (equal); Writing – review & editing (equal). **Zhongrui Liu:** Conceptualization (equal); Investigation (equal); Methodology (equal); Writing – review & editing (supporting). **Sankar Raju Narayanasamy:** Software (lead); Visualization (supporting); Writing – review & editing (supporting). **Megan L. Shelby:** Formal analysis (equal); Investigation (equal); Resources (equal); Writing – review & editing (supporting). **Nicholas Chan:** Investigation (supporting). **Matthew A. Coleman:** Supervision (equal). **Matthias Frank:** Conceptualization (equal); Funding acquisition (equal); Methodology (equal); Supervision (equal); Writing – review & editing (equal). **Tonya L. Kuhl:** Conceptualization (equal); Funding acquisition (equal); Methodology (equal); Supervision (equal); Writing – review & editing (equal).

DATA AVAILABILITY

Raw data were generated at both Stanford Synchrotron Radiation Lightsource (SSRL) and Linac Coherent Light Source (LCLS). The derived data that support the findings of this study are available within this article and its supplementary material, the article by Liu *et al.*, or is available from the corresponding author upon reasonable request.

REFERENCES

[1]H. M. Berman, "The protein data bank," Nucleic Acids Res. **28**(1), 235–242 (2000).
[2]Y. Shi, "A glimpse of structural biology through x-ray crystallography," Cell **159**(5), 995–1014 (2014).
[3]J. M. Holton and K. A. Frankel, "The minimum crystal size needed for a complete diffraction data set," Acta Crystallogr., Sect. D: Biol. Crystallogr. **66**(4), 393–408 (2010).
[4]J. C. H. Spence, U. Weierstall, and H. N. Chapman, "X-ray lasers for structural and dynamic biology," Rep. Prog. Phys. **75**(10), 102601 (2012).
[5]T. R. M. Barends, B. Stauch, V. Cherezov, and I. Schlichting, "Serial femtosecond crystallography," Nat. Rev. Methods Primers **2**(1), 59 (2022).
[6]H. N. Chapman, P. Fromme, A. Barty, T. A. White, R. A. Kirian, A. Aquila, M. S. Hunter, J. Schulz, D. P. DePonte, U. Weierstall, R. B. Doak, F. R. N. C. Maia, A. V. Martin, I. Schlichting, L. Lomb, N. Coppola, R. L. Shoeman, S. W. Epp, R. Hartmann, D. Rolles, A. Rudenko, L. Foucar, N. Kimmel, G. Weidenspointner, P. Holl, M. Liang, M. Barthelmess, C. Caleman, S. Boutet, M. J. Bogan, J. Krzywinski, C. Bostedt, S. Bajt, L. Gumprecht, B. Rudek, B. Erk, C. Schmidt, A. Hömke, C. Reich, D. Pietschner, L. Strüder, G. Hauser, H. Gorke, J. Ullrich, S. Herrmann, G. Schaller, F. Schopper, H. Soltau, K.-U. Kühnel, M. Messerschmidt, J. D. Bozek, S. P. Hau-Riege, M. Frank, C. Y. Hampton, R. G. Sierra, D. Starodub, G. J. Williams, J. Hajdu, N. Timneanu, M. M. Seibert, J. Andreasson, A. Rocker, O. Jönsson, M. Svenda, S. Stern, K. Nass, R. Andritschke, C.-D. Schröter, F. Krasniqi, M. Bott, K. E. Schmidt, X. Wang, I. Grotjohann, J. M. Holton, T. R. M. Barends, R. Neutze, S. Marchesini, R. Fromme, S. Schorb, D. Rupp, M. Adolph, T. Gorkhover, I. Andersson, H. Hirsemann, G. Potdevin, H. Graafsma, B. Nilsson, and J. C. H. Spence, "Femtosecond x-ray protein nanocrystallography," Nature **470**(7332), 73–77 (2011).
[7]L. C. Johansson, B. Stauch, A. Ishchenko, and V. Cherezov, "A bright future for serial femtosecond crystallography with XFELs," Trends Biochem. Sci. **42**(9), 749–762 (2017).
[8]M. Fischer, "Macromolecular room temperature crystallography," Q. Rev. Biophys. **54**, e1 (2021).
[9]K. Hirata, K. Shinzawa-Itoh, N. Yano, S. Takemura, K. Kato, M. Hatanaka, K. Muramoto, T. Kawahara, T. Tsukihara, E. Yamashita, K. Tono, G. Ueno, T. Hikima, H. Murakami, Y. Inubushi, M. Yabashi, T. Ishikawa, M. Yamamoto, T. Ogura, H. Sugimoto, J.-R. Shen, S. Yoshikawa, and H. Ago, "Determination of damage-free crystal structure of an x-ray–sensitive protein using an XFEL," Nat. Methods **11**(7), 734–736 (2014).
[10]W. Liu, D. Wacker, C. Gati, G. W. Han, D. James, D. Wang, G. Nelson, U. Weierstall, V. Katritch, A. Barty, N. A. Zatsepin, D. Li, M. Messerschmidt, S. Boutet, G. J. Williams, J. E. Koglin, M. M. Seibert, C. Wang, S. T. A. Shah, S. Basu, R. Fromme, C. Kupitz, K. N. Rendek, I. Grotjohann, P. Fromme, R. A. Kirian, K. R. Beyerlein, T. A. White, H. N. Chapman, M. Caffrey, J. C. H. Spence, R. C. Stevens, and V. Cherezov, "Serial femtosecond crystallography of G protein–coupled receptors," Science **342**(6165), 1521–1524 (2013).
[11]F. Z. Zhao, B. Zhang, E. K. Yan, B. Sun, Z. J. Wang, J. H. He, and D. C. Yin, "A guide to sample delivery systems for serial crystallography," FEBS J. **286**(22), 4402–4417 (2019).
[12]A. Echelmeier, M. Sonker, and A. Ros, "Microfluidic sample delivery for serial crystallography using XFELs," Anal. Bioanal. Chem. **411**(25), 6535–6547 (2019).
[13]M. L. Grünbein and G. Nass Kovacs, "Sample delivery for serial crystallography at free-electron lasers and synchrotrons," Acta Crystallogr., Sect. D: Struct. Biol. **75**(2), 178–191 (2019).
[14]R. G. Sierra, U. Weierstall, D. Oberthuer, M. Sugahara, E. Nango, S. Iwata, and A. Meents, "Sample delivery techniques for serial crystallography," in *X-ray Free Electron Lasers*, edited by S. Boutet, P. Fromme, and M. S. Hunter (Springer International Publishing, Cham, 2018), pp. 109–184.
[15]I. Martiel, H. M. Müller-Werkmeister, and A. E. Cohen, "Strategies for sample delivery for femtosecond crystallography," Acta Crystallogr., Sect. D: Struct. Biol. **75**(2), 160–177 (2019).
[16]R. Cheng, "Towards an optimal sample delivery method for serial crystallography at XFEL," Crystals **10**(3), 215 (2020).
[17]S. R. Narayanasamy, R. Vasireddi, H.-Y. N. Holman, and M. Trebbin, "A sui generis whipping-instability-based self-sequencing multi-monodisperse 2D spray from an anisotropic microfluidic liquid jet device," Cell Rep. Phys. Sci. **4**(1), 101221 (2023).
[18]J. Knoška, L. Adriano, S. Awel, K. R. Beyerlein, O. Yefanov, D. Oberthuer, G. E. Peña Murillo, N. Roth, I. Sarrou, P. Villanueva-Perez, M. O. Wiedorn, F. Wilde, S. Bajt, H. N. Chapman, and M. Heymann, "Ultracompact 3D microfluidics for time-resolved structural biology," Nat. Commun. **11**(1), 657 (2020).
[19]P. Berntsen, C. Darmanin, E. Balaur, L. Flueckiger, A. Kozlov, F. G. Roque, P. Adams, J. Binns, D. Wells, M. Hadian Jazi, S. Saha, A. Hawley, T. Ryan, S. Mudie, N. Kirby, B. Abbey, and A. V. Martin, "Stability, flow alignment and a phase transition of the lipidic cubic phase during continuous flow injection," J. Colloid Interface Sci. **611**, 588–598 (2022).
[20]D. J. Wells, P. Berntsen, E. Balaur, C. M. Kewish, P. Adams, A. Aquila, J. Binns, S. Boutet, H. Broomhall, C. Caleman, A. Christofferson, C. E. Conn, C. Dahlqvist, L. Flueckiger, F. Gian Roque, T. L. Greaves, M. Hejazian, M. Hunter, M. Hadian Jazi, H. O. Jönsson, S. K. Pathirannahalage, R. A. Kirian, A. Kozlov, R. P. Kurta, H. Marman, D. Mendez, A. Morgan, K. Nugent, D. Oberthuer, H. Quiney, J. Reinhardt, S. Saha, J. A. Sellberg, R. Sierra, M. Wiedorn, B. Abbey, A. V. Martin, and C. Darmanin, "Observations of phase changes in monoolein during high viscous injection," J. Synchrotron Radiat. **29**(3), 602–614 (2022).
[21]M. L. Grünbein, L. Foucar, A. Gorel, M. Hilpert, M. Kloos, K. Nass, G. N. Kovacs, C. M. Roome, R. L. Shoeman, M. Stricker, S. Carbajo, W. Colocho, S. Gilevich, M. Hunter, J. Lewandowski, A. Lutman, J. E. Koglin, T. J. Lane, T. van Driel, J. Sheppard, S. L. Vetter, J. L. Turner, R. B. Doak, T. R. M. Barends, S. Boutet, A. L. Aquila, F.-J. Decker, I. Schlichting, and C. A. Stan, "Observation of shock-induced protein crystal damage during megahertz serial femtosecond crystallography," Phys. Rev. Res. **3**(1), 013046 (2021).
[22]F. D. Fuller, S. Gul, R. Chatterjee, E. S. Burgie, I. D. Young, H. Lebrette, V. Srinivas, A. S. Brewster, T. Michels-Clark, J. A. Clinger, B. Andi, M. Ibrahim, E. Pastor, C. De Lichtenberg, R. Hussein, C. J. Pollock, M. Zhang, C. A. Stan, T. Kroll, T. Fransson, C. Weninger, M. Kubin, P. Aller, L. Lassalle, P. Bräuer, M. D. Miller, M. Amin, S. Koroidov, C. G. Roessler, M. Allaire, R. G. Sierra, P. T. Docker, J. M. Glownia, S. Nelson, J. E. Koglin, D. Zhu, M. Chollet, S. Song, H. Lemke, M. Liang, D. Sokaras, R. Alonso-Mori, A. Zouni, J. Messinger, U. Bergmann, A. K. Boal, J. M. Bollinger, C. Krebs, M. Högbom, G. N. Phillips, R. D. Vierstra, N. K. Sauter, A. M. Orville, J. Kern, V. K. Yachandra, and J. Yano, "Drop-on-demand sample delivery for studying biocatalysts in action at x-ray free-electron lasers," Nat. Methods **14**(4), 443–449 (2017).
[23]A. Henkel, M. Galchenkova, J. Maracke, O. Yefanov, B. Klopprogge, J. Hakanpää, J. R. Mesters, H. N. Chapman, and D. Oberthuer, "JINXED: Just in time crystallization for easy structure determination of biological macromolecules," IUCrJ **10**(3), 253–260 (2023).
[24]K. A. Zielinski, A. Prester, H. Andaleeb, S. Bui, O. Yefanov, L. Catapano, A. Henkel, M. O. Wiedorn, O. Lorbeer, E. Crosas, J. Meyer, V. Mariani, M. Domaracky, T. A. White, H. Fleckenstein, I. Sarrou, N. Werner, C. Betzel, H. Rohde, M. Aepfelbacher, H. N. Chapman, M. Perbandt, R. A. Steiner, and D. Oberthuer, "Rapid and efficient room-temperature serial synchrotron crystallography using the CFEL TapeDrive," IUCrJ **9**(6), 778–791 (2022).
[25]R. G. Sierra, C. Gati, H. Laksmono, E. H. Dao, S. Gul, F. Fuller, J. Kern, R. Chatterjee, M. Ibrahim, A. S. Brewster, I. D. Young, T. Michels-Clark, A. Aquila, M. Liang, M. S. Hunter, J. E. Koglin, S. Boutet, E. A. Junco, B. Hayes, M. J. Bogan, C. Y. Hampton, E. V. Puglisi, N. K. Sauter, C. A. Stan, A. Zouni, J. Yano, V. K. Yachandra, S. M. Soltis, J. D. Puglisi, and H. DeMirci, "Concentric-flow electrokinetic injector enables serial crystallography of ribosome and photosystem II," Nat. Methods **13**(1), 59–62 (2016).
[26]E. H. Dao, F. Poitevin, R. G. Sierra, C. Gati, Y. Rao, H. I. Ciftci, F. Akşit, A. McGurk, T. Obrinski, P. Mgbam, B. Hayes, C. De Lichtenberg, F. Pardo-Avila, N. Corsepius, L. Zhang, M. H. Seaberg, M. S. Hunter, M. Liang, J. E. Koglin, S. Wakatsuki, and H. Demirci, "Structure of the 30S ribosomal decoding complex at ambient temperature," RNA **24**(12), 1667–1676 (2018).

[27]D. P. DePonte, U. Weierstall, K. Schmidt, J. Warner, D. Starodub, J. C. H. Spence, and R. B. Doak, "Gas dynamic virtual nozzle for generation of microscopic droplet streams," J. Phys. D: Appl. Phys. **41**(19), 195505 (2008).
[28]U. Weierstall, "Liquid sample delivery techniques for serial femtosecond crystallography," Philos. Trans. R. Soc., B **369**(1647), 20130337 (2014).
[29]M. Vakili, R. Vasireddi, P. V. Gwozdz, D. C. F. Monteiro, M. Heymann, R. H. Blick, and M. Trebbin, "Microfluidic polyimide gas dynamic virtual nozzles for serial crystallography," Rev. Sci. Instrum. **91**(8), 085108 (2020).
[30]R. Fromme, A. Ishchenko, M. Metz, S. R. Chowdhury, S. Basu, S. Boutet, P. Fromme, T. A. White, A. Barty, J. C. H. Spence, U. Weierstall, W. Liu, and V. Cherezov, "Serial femtosecond crystallography of soluble proteins in lipidic cubic phase," IUCrJ **2**(5), 545–551 (2015).
[31]A. E. Cohen, S. M. Soltis, A. González, L. Aguila, R. Alonso-Mori, C. O. Barnes, E. L. Baxter, W. Brehmer, A. S. Brewster, A. T. Brunger, G. Calero, J. F. Chang, M. Chollet, P. Ehrensberger, T. L. Eriksson, Y. Feng, J. Hattne, B. Hedman, M. Hollenbeck, J. M. Holton, S. Keable, B. K. Kobilka, E. G. Kovaleva, A. C. Kruse, H. T. Lemke, G. Lin, A. Y. Lyubimov, A. Manglik, I. I. Mathews, S. E. McPhillips, S. Nelson, J. W. Peters, N. K. Sauter, C. A. Smith, J. Song, H. P. Stevenson, Y. Tsai, M. Uervirojnangkoorn, V. Vinetsky, S. Wakatsuki, W. I. Weis, O. A. Zadvornyy, O. B. Zeldin, D. Zhu, and K. O. Hodgson, "Goniometer-based femtosecond crystallography with x-ray free electron lasers," Proc. Natl. Acad. Sci. U.S.A. **111**(48), 17122–17127 (2014).
[32]D. Gilbile, M. L. Shelby, A. Y. Lyubimov, J. L. Wierman, D. C. F. Monteiro, A. E. Cohen, S. Russi, M. A. Coleman, M. Frank, and T. L. Kuhl, "Plug-and-play polymer microfluidic chips for hydrated, room temperature, fixed-target serial crystallography," Lab Chip **21**(24), 4831–4845 (2021).
[33]R. Vasireddi, A. Gardais, and L. M. G. Chavas, "Manufacturing of ultra-thin x-ray-compatible COC microfluidic devices for optimal *in situ* macromolecular crystallography experiments," Micromachines **13**(8), 1365 (2022).
[34]T. Kimura, Y. Joti, A. Shibuya, C. Song, S. Kim, K. Tono, M. Yabashi, M. Tamakoshi, T. Moriya, T. Oshima, T. Ishikawa, Y. Bessho, and Y. Nishino, "Imaging live cell in micro-liquid enclosure by x-ray laser diffraction," Nat. Commun. **5**(1), 3052 (2014).
[35]M. S. Hunter, B. Segelke, M. Messerschmidt, G. J. Williams, N. A. Zatsepin, A. Barty, W. H. Benner, D. B. Carlson, M. Coleman, A. Graf, S. P. Hau-Riege, T. Pardini, M. M. Seibert, J. Evans, S. Boutet, and M. Frank, "Fixed-target protein serial microcrystallography with an x-ray free electron laser," Sci. Rep. **4**(1), 6026 (2014).
[36]S. Horrell, D. Axford, N. E. Devenish, A. Ebrahim, M. A. Hough, D. A. Sherrell, S. L. S. Storm, I. Tews, J. A. R. Worrall, and R. L. Owen, "Fixed target serial data collection at diamond light source," J. Vis. Exp. **2021**(168), 62200 (2021).
[37]M. L. Shelby, D. Gilbile, T. D. Grant, C. Seuring, B. W. Segelke, W. He, A. C. Evans, T. Pakendorf, P. Fischer, M. S. Hunter, A. Batyuk, M. Barthelmess, A. Meents, M. A. Coleman, T. L. Kuhl, and M. Frank, "A fixed-target platform for serial femtosecond crystallography in a hydrated environment," IUCrJ **7**(1), 30–41 (2020).
[38]A. Y. Lyubimov, T. D. Murray, A. Koehl, I. E. Araci, M. Uervirojnangkoorn, O. B. Zeldin, A. E. Cohen, S. M. Soltis, E. L. Baxter, A. S. Brewster, N. K. Sauter, A. T. Brunger, and J. M. Berger, "Capture and x-ray diffraction studies of protein microcrystals in a microfluidic trap array," Acta Crystallogr., Sect. D: Biol. Crystallogr. **71**(4), 928–940 (2015).
[39]J. Lieske, M. Cerv, S. Kreida, D. Komadina, J. Fischer, M. Barthelmess, P. Fischer, T. Pakendorf, O. Yefanov, V. Mariani, T. Seine, B. H. Ross, E. Crosas, O. Lorbeer, A. Burkhardt, T. J. Lane, S. Guenther, J. Bergtholdt, S. Schoen, S. Törnroth-Horsefield, H. N. Chapman, and A. Meents, "On-chip crystallization for serial crystallography experiments and on-chip ligand-binding studies," IUCrJ **6**(4), 714–728 (2019).
[40]T. D. Murray, A. Y. Lyubimov, C. M. Ogata, H. Vo, M. Uervirojnangkoorn, A. T. Brunger, and J. M. Berger, "A high-transparency, micro-patternable chip for x-ray diffraction analysis of microcrystals under native growth conditions," Acta Crystallogr., Sect. D: Biol. Crystallogr. **71**(10), 1987–1997 (2015).
[41]P. Roedig, I. Vartiainen, R. Duman, S. Panneerselvam, N. Stübe, O. Lorbeer, M. Warmer, G. Sutton, D. I. Stuart, E. Weckert, C. David, A. Wagner, and A. Meents, "A micro-patterned silicon chip as sample holder for macromolecular crystallography experiments with minimal background scattering," Sci. Rep. **5**(1), 10451 (2015).
[42]J. L. Wierman, O. Paré-Labrosse, A. Sarracini, J. E. Besaw, M. J. Cook, S. Oghbaey, H. Daoud, P. Mehrabi, I. Kriksunov, A. Kuo, D. J. Schuller, S. Smith, O. P. Ernst, D. M. E. Szebenyi, S. M. Gruner, R. J. D. Miller, and A. D. Finke, "Fixed-target serial oscillation crystallography at room temperature," IUCrJ **6**(2), 305–316 (2019).
[43]R. L. Owen, D. Axford, D. A. Sherrell, A. Kuo, O. P. Ernst, E. C. Schulz, R. J. D. Miller, and H. M. Mueller-Werkmeister, "Low-dose fixed-target serial synchrotron crystallography," Acta Crystallogr., Sect. D: Struct. Biol. **73**(4), 373–378 (2017).
[44]M. Liang, L. Yu, Z. Wang, H. Zhou, Y. Zhang, Q. Wang, and J. He, "Novel combined crystallization plate for high-throughput crystal screening and *in situ* data collection at a crystallography beamline," Acta Crystallogr., Sect. F: Struct. Biol. Commun. **77**(9), 319–327 (2021).
[45]K. H. Nam, J. Kim, and Y. Cho, "Polyimide mesh-based sample holder with irregular crystal mounting holes for fixed-target serial crystallography," Sci. Rep. **11**(1), 13115 (2021).
[46]C. Mueller, A. Marx, S. W. Epp, Y. Zhong, A. Kuo, A. R. Balo, J. Soman, F. Schotte, H. T. Lemke, R. L. Owen, E. F. Pai, A. R. Pearson, J. S. Olson, P. A. Anfinrud, O. P. Ernst, and R. J. Dwayne Miller, "Fixed target matrix for femtosecond time-resolved and *in situ* serial micro-crystallography," Struct. Dyn. **2**(5), 054302 (2015).
[47]A. Karpik, I. Martiel, P. M. Kristiansen, and C. Padeste, "Fabrication of ultra-thin suspended polymer membranes as supports for serial protein crystallography," Micro Nano Eng. **7**, 100053 (2020).
[48]I. Chaussavoine, T. Isabet, R. Lener, P. Montaville, R. Vasireddi, and L. M. G. Chavas, "Implementation of wedged-serial protein crystallography at PROXIMA-1," J. Synchrotron Radiat. **29**(2), 439–446 (2022).
[49]Y. Gicquel, R. Schubert, S. Kapis, G. Bourenkov, T. Schneider, M. Perbandt, C. Betzel, H. N. Chapman, and M. Heymann, "Microfluidic chips for *in situ* crystal x-ray diffraction and *in situ* dynamic light scattering for serial crystallography," J. Vis. Exp. **2018**(134), 57133 (2018).
[50]R. De Wijn, O. Hennig, J. Roche, S. Engilberge, K. Rollet, P. Fernandez-Millan, K. Brillet, H. Betat, M. Mörl, A. Roussel, E. Girard, C. Mueller-Dieckmann, G. C. Fox, V. Olieric, J. A. Gavira, B. Lorber, and C. Sauter, "A simple and versatile microfluidic device for efficient biomacromolecule crystallization and structural analysis by serial crystallography," IUCrJ **6**(3), 454–464 (2019).
[51]M. Maeki, S. Ito, R. Takeda, G. Ueno, A. Ishida, H. Tani, M. Yamamoto, and M. Tokeshi, "Room-temperature crystallography using a microfluidic protein crystal array device and its application to protein–ligand complex structure analysis," Chem. Sci. **11**(34), 9072–9087 (2020).
[52]S. Saha, C. Özden, A. Samkutty, S. Russi, A. Cohen, M. M. Stratton, and S. L. Perry, "Polymer-based microfluidic device for on-chip counter-diffusive crystallization and *in situ* x-ray crystallography at room temperature," Lab Chip **23**(8), 2075–2090 (2023).
[53]F.-Z. Zhao, Z.-J. Wang, Q.-J. Xiao, L. Yu, B. Sun, Q. Hou, L.-L. Chen, H. Liang, H. Wu, W.-H. Guo, J.-H. He, Q.-S. Wang, and D.-C. Yin, "Microfluidic rotating-target device capable of three-degrees-of-freedom motion for efficient *in situ* serial synchrotron crystallography," J. Synchrotron Radiat. **30**(2), 347–358 (2023).
[54]N. Junius, S. Jaho, Y. Sallaz-Damaz, F. Borel, J.-B. Salmon, and M. Budayova-Spano, "A microfluidic device for both on-chip dialysis protein crystallization and *in situ* x-ray diffraction," Lab Chip **20**(2), 296–310 (2020).
[55]S. Sui and S. L. Perry, "Microfluidics: From crystallization to serial time-resolved crystallography," Struct. Dyn. **4**(3), 032202 (2017).
[56]C. L. Hansen, E. Skordalakes, J. M. Berger, and S. R. Quake, "A robust and scalable microfluidic metering method that allows protein crystal growth by free interface diffusion," Proc. Natl. Acad. Sci. U.S.A. **99**(26), 16531–16536 (2002).

[57]S. Jaho, N. Junius, F. Borel, Y. Sallaz-Damaz, J.-B. Salmon, and M. Budayova-Spano, "Crystallization of proteins on chip by microdialysis for *in situ* x-ray diffraction studies," J. Vis. Exp. **2021**(170), 61660 (2021).
[58]A. M. Popov, P. V. Dorovatovskii, D. A. Mamichev, M. A. Marchenkova, and A. Y. Nikolaeva, "Development of a microfluidic chip for protein crystallization by the microbatch method," Crystallogr. Rep. **64**(2), 282–286 (2019).
[59]S. L. Perry, G. W. Roberts, J. D. Tice, R. B. Gennis, and P. J. A. Kenis, "Microfluidic generation of lipidic mesophases for membrane protein crystallization," Cryst. Growth Des. **9**(6), 2566–2569 (2009).
[60]D. S. Khvostichenko, J. M. Schieferstein, A. S. Pawate, P. D. Laible, and P. J. A. Kenis, "X-ray transparent microfluidic chip for mesophase-based crystallization of membrane proteins and on-chip structure determination," Cryst. Growth Des. **14**(10), 4886–4890 (2014).
[61]I. Martiel, J. H. Beale, A. Karpik, C.-Y. Huang, L. Vera, N. Olieric, M. Wranik, C.-J. Tsai, J. Mühle, O. Aurelius, J. John, M. Högbom, M. Wang, M. Marsh, and C. Padeste, "Versatile microporous polymer-based supports for serial macromolecular crystallography," Acta Crystallogr., Sect. D: Struct. Biol. **77**(9), 1153–1167 (2021).
[62]J. Wang, Y. Zhou, H. Qiu, H. Huang, C. Sun, J. Xi, and Y. Huang, "A chip-to-chip nanoliter microfluidic dispenser," Lab Chip **9**(13), 1831 (2009).
[63]G. Li, Q. Chen, J. Li, X. Hu, and J. Zhao, "A compact disk-like centrifugal microfluidic system for high-throughput nanoliter-scale protein crystallization screening," Anal. Chem. **82**(11), 4362–4369 (2010).
[64]Z. Liu, K. Gu, M. Shelby, D. Gilbile, A. Lyubimov, S. Russi, A. Cohen, S. R. Narayanasamy, S. Botha, C. Kupitz, R. Sierra, F. Poitevin, A. Gilardi, S. Lisova, M. Coleman, M. Frank, and T. Kuhl, "A user-friendly plug-and-play cyclic olefin copolymer-based microfluidic chip for room-temperature, fixed-target serial crystallography," Acta Crystallogr., Sect. D: Struct. Biol. (published online 2023).
[65]C. Kupitz, I. Grotjohann, C. E. Conrad, S. Roy-Chowdhury, R. Fromme, and P. Fromme, "Microcrystallization techniques for serial femtosecond crystallography using photosystem II from *Thermosynechococcus elongatus* as a model system," Philos. Trans. R. Soc., B **369**(1647), 20130316 (2014).
[66]J. H. Beale, R. Bolton, S. A. Marshall, E. V. Beale, S. B. Carr, A. Ebrahim, T. Moreno-Chicano, M. A. Hough, J. A. R. Worrall, I. Tews, and R. L. Owen, "Successful sample preparation for serial crystallography experiments," J. Appl. Crystallogr. **52**(6), 1385–1396 (2019).
[67]C. Stohrer, S. Horrell, S. Meier, M. Sans, D. Von Stetten, M. Hough, A. Goldman, D. C. F. Monteiro, and A. R. Pearson, "Homogeneous batch microcrystallization of proteins from ammonium sulfate," Acta Crystallogr., Sect. D: Struct. Biol. **77**(2), 194–204 (2021).
[68]N. E. Chayen and E. Saridakis, "Protein crystallization: From purified protein to diffraction-quality crystal," Nat. Methods **5**(2), 147–153 (2008).
[69]E. C. Schulz, B. A. Yorke, A. R. Pearson, and P. Mehrabi, "Best practices for time-resolved serial synchrotron crystallography," Acta Crystallogr., Sect. D: Struct. Biol. **78**(1), 14–29 (2022).
[70]R. L. Shoeman, E. Hartmann, and I. Schlichting, "Growing and making nano- and microcrystals," Nat. Protoc. **18**((3), 854–882 (2023).
[71]M. Maeki, S. Yamazaki, R. Takeda, A. Ishida, H. Tani, and M. Tokeshi, "Real-time measurement of protein crystal growth rates within the microfluidic device to understand the microspace effect," ACS Omega **5**(28), 17199–17206 (2020).
[72]K. Nam, "Sample delivery media for serial crystallography," Int. J. Mol. Sci. **20**(5), 1094 (2019).
[73]D. Cohn, G. Lando, A. Sosnik, S. Garty, and A. Levi, "PEO–PPO–PEO-based poly(ether ester urethane)s as degradable reverse thermo-responsive multiblock copolymers," Biomaterials **27**(9), 1718–1727 (2006).
[74]G. Kovácsová, M. L. Grünbein, M. Kloos, T. R. M. Barends, R. Schlesinger, J. Heberle, W. Kabsch, R. L. Shoeman, R. B. Doak, and I. Schlichting, "Viscous hydrophilic injection matrices for serial crystallography," IUCrJ **4**(4), 400–410 (2017).
[75]J. Park, Y. Joti, T. Ishikawa, and C. Song, "Monte Carlo study for optimal conditions in single-shot imaging with femtosecond x-ray laser pulses," Appl. Phys. Lett. **103**(26), 264101 (2013).
[76]T. Bergfors, "Seeds to crystals," J. Struct. Biol. **142**(1), 66–76 (2003).
[77]J. Sanchez-Weatherby, M. W. Bowler, J. Huet, A. Gobbo, F. Felisaz, B. Lavault, R. Moya, J. Kadlec, R. B. G. Ravelli, and F. Cipriani, "Improving diffraction by humidity control: A novel device compatible with x-ray beamlines," Acta Crystallogr., Sect. D: Biol. Crystallogr. **65**(12), 1237–1246 (2009).
[78]I. Russo Krauss, F. Sica, C. A. Mattia, and A. Merlino, "Increasing the x-ray diffraction power of protein crystals by dehydration: The case of bovine serum albumin and a survey of literature data," Int. J. Mol. Sci. **13**(3), 3782–3800 (2012).
[79]M. W. Bowler, M. G. Montgomery, A. G. W. Leslie, and J. E. Walker, "Reproducible improvements in order and diffraction limit of crystals of bovine mitochondrial F_1-ATPase by controlled dehydration," Acta Crystallogr., Sect. D: Biol. Crystallogr. **62**(9), 991–995 (2006).
[80]R. G. Sierra, A. Batyuk, Z. Sun, A. Aquila, M. S. Hunter, T. J. Lane, M. Liang, C. H. Yoon, R. Alonso-Mori, R. Armenta, J.-C. Castagna, M. Hollenbeck, T. O. Osier, M. Hayes, J. Aldrich, R. Curtis, J. E. Koglin, T. Rendahl, E. Rodriguez, S. Carbajo, S. Guillet, R. Paul, P. Hart, K. Nakahara, G. Carini, H. DeMirci, E. H. Dao, B. M. Hayes, Y. P. Rao, M. Chollet, Y. Feng, F. D. Fuller, C. Kupitz, T. Sato, M. H. Seaberg, S. Song, T. B. van Driel, H. Yavas, D. Zhu, A. E. Cohen, S. Wakatsuki, and S. Boutet, "The macromolecular femtosecond crystallography instrument at the linac coherent light source," J. Synchrotron Radiat. **26**(2), 346–357 (2019).
[81]J.-Z. Zhang, J. K. Lam, C. F. Wood, B.-T. Chu, and R. K. Chang, "Explosive vaporization of a large transparent droplet irradiated by a high intensity laser," Appl. Opt. **26**(22), 4731 (1987).
[82]G. Blaj, M. Liang, A. L. Aquila, P. R. Willmott, J. E. Koglin, R. G. Sierra, J. S. Robinson, S. Boutet, and C. A. Stan, "Generation of high-intensity ultrasound through shock propagation in liquid jets," Phys. Rev. Fluids **4**(4), 043401 (2019).
[83]C. A. Stan, D. Milathianaki, H. Laksmono, R. G. Sierra, T. A. McQueen, M. Messerschmidt, G. J. Williams, J. E. Koglin, T. J. Lane, M. J. Hayes, S. A. H. Guillet, M. Liang, A. L. Aquila, P. R. Willmott, J. S. Robinson, K. L. Gumerlock, S. Botha, K. Nass, I. Schlichting, R. L. Shoeman, H. A. Stone, and S. Boutet, "Liquid explosions induced by x-ray laser pulses," Nat. Phys. **12**(10), 966–971 (2016).
[84]J. Wang, "Destruction-and-diffraction by x-ray free-electron laser: Diffraction-before-destruction or destruction-and-diffraction?," Protein Sci. **25**(9), 1585–1592 (2016).
[85]J. Wang, "Oxygen additions in serial femtosecond crystallographic protein structures: Oxygen additions in SFX protein structures," Protein Sci. **25**(10), 1797–1802 (2016).
[86]S. M. Seltzer, "Calculation of photon mass energy-transfer and mass energy-absorption coefficients," Radiat. Res. **136**(2), 147 (1993).
[87]B. G. Abdallah, N. A. Zatsepin, S. Roy-Chowdhury, J. Coe, C. E. Conrad, K. Dörner, R. G. Sierra, H. P. Stevenson, F. Camacho-Alanis, T. D. Grant, G. Nelson, D. James, G. Calero, R. M. Wachter, J. C. H. Spence, U. Weierstall, P. Fromme, and A. Ros, "Microfluidic sorting of protein nanocrystals by size for x-ray free-electron laser diffraction," Struct. Dyn. **2**(4), 041719 (2015).
[88]C.-Y. Huang, N. Meier, M. Caffrey, M. Wang, and V. Olieric, "3D-Printed holders for *in meso in situ* fixed-target serial x-ray crystallography," J. Appl. Crystallogr. **53**(3), 854–859 (2020).
[89]W. Liu, D. Wacker, C. Wang, E. Abola, and V. Cherezov, "Femtosecond crystallography of membrane proteins in the lipidic cubic phase," Philos. Trans. R. Soc., B **369**(1647), 20130314 (2014).
[90]E. L. Baxter, L. Aguila, R. Alonso-Mori, C. O. Barnes, C. A. Bonagura, W. Brehmer, A. T. Brunger, G. Calero, T. T. Caradoc-Davies, R. Chatterjee, W. F. Degrado, J. S. Fraser, M. Ibrahim, J. Kern, B. K. Kobilka, A. C. Kruse, K. M. Larsson, H. T. Lemke, A. Y. Lyubimov, A. Manglik, S. E. McPhillips, E. Norgren, S. S. Pang, S. M. Soltis, J. Song, J. Thomaston, Y. Tsai, W. I. Weis, R. A. Woldeyes, V. Yachandra, J. Yano, A. Zouni, and A. E. Cohen, "High-density grids for efficient data collection from multiple crystals," Acta Crystallogr., Sect. D: Struct. Biol. **72**(1), 2–11 (2016).
[91]J. A. Gavira, I. Rodriguez-Ruiz, S. Martinez-Rodriguez, S. Basu, S. Teychené, A. A. McCarthy, and C. Mueller-Dieckman, "Attaining atomic resolution from *in*

situ data collection at room temperature using counter-diffusion-based low-cost microchips," Acta Crystallogr., Sect. D: Struct. Biol. **76**(8), 751–758 (2020).
[92]F. Li and R. Lakerveld, "Influence of alternating electric fields on protein crystallization in microfluidic devices with patterned electrodes in a parallel-plate configuration," Cryst. Growth Des. **17**(6), 3062–3070 (2017).
[93]A. Tolstikova, M. Levantino, O. Yefanov, V. Hennicke, P. Fischer, J. Meyer, A. Mozzanica, S. Redford, E. Crosas, N. L. Opara, M. Barthelmess, J. Lieske, D. Oberthuer, E. Wator, I. Mohacsi, M. Wulff, B. Schmitt, H. N. Chapman, and A. Meents, "1 KHz fixed-target serial crystallography using a multilayer monochromator and an integrating pixel detector," IUCrJ **6**(5), 927–937 (2019).